Turbulent structure of high-density suspensions formed under waves

Michael P. Lamb
Department of Earth and Planetary Science, University of California, Berkeley, California, USA

Eric D'Asaro
Applied Physics Laboratory, University of Washington, Seattle, Washington, USA

Jeffrey D. Parsons
School of Oceanography, University of Washington, Seattle, Washington, USA

Received 27 February 2004; revised 6 July 2004; accepted 22 September 2004; published 22 December 2004.

[1] We performed a series of laboratory experiments on the interactions between turbulent wave boundary layers and a predominantly silt-sized sediment bed. Under a wide range of wave conditions similar to those observed on storm-dominated midshelf environments we produced quasi-steady high-density benthic suspensions. These suspensions were turbulent, while containing large near-bed concentrations of suspended sediment (17–80 g/L), and were separated from the upper water column by a lutocline. Detailed measurements of the vertical structure of velocity, turbulence, and sediment concentration revealed that the wave boundary layer, while typically >1 cm thick in sediment-free conditions, was reduced substantially in size, often to <3 mm, with the addition of suspendible sediment. This likely resulted from sediment-induced stratification that limited vertical mixing of momentum. Despite boundary layer reduction the flows were able to support high-density suspensions as thick as 8 cm because turbulent energy was transported upward from this thin but highly energetic near-bed region. Standard formulations of the Richardson number for shear flows are not applicable to our experiments since the suspensions were supported from transported rather than locally produced turbulence. *INDEX TERMS:* 3022 Marine Geology and Geophysics: Marine sediments—processes and transport; 4211 Oceanography: General: Benthic boundary layers; 4558 Oceanography: Physical: Sediment transport; 4560 Oceanography: Physical: Surface waves and tides (1255); 4568 Oceanography: Physical: Turbulence, diffusion, and mixing processes; *KEYWORDS:* wave boundary layer, oscillatory, high-density suspension, fluid mud, turbulent kinetic energy budget

Citation: Lamb, M. P., E. D'Asaro, and J. D. Parsons (2004), Turbulent structure of high-density suspensions formed under waves, *J. Geophys. Res.*, *109*, C12026, doi:10.1029/2004JC002355.

1. Introduction

[2] Several recent studies have documented high-density benthic suspensions (HDS), often referred to as fluid mud, on wave-dominated continental shelves during storm conditions (e.g., Eel shelf, California [*Ogston et al.*, 2000; *Traykovski et al.*, 2000]). HDS typically have sediment concentrations in excess of 10 g/L and are defined by the presence of a lutocline, a sharp break in concentration separating the suspension from the clear fluid above. It has been argued that the formation and stabilization of HDS in storm-dominated shelf environments are genetically linked to the dynamics and size of the wave boundary layer [*Friedrichs et al.*, 2000; *Wright et al.*, 2001]. HDS, when advected by a current or by the force of gravity, might be responsible for most of the cross-shelf sediment transport and strata formation on the Eel shelf [*Traykovski et al.*, 2000].

[3] Despite recent field studies the dynamics of HDS remain unclear because detailed quantitative measurements in a turbulent wave boundary layer in the presence of high concentrations of suspended sediment are difficult. A laboratory flume provides an opportunity to make visual and quantitative measurements of HDS under controlled conditions. Unfortunately, little work has been done on turbulent wave boundary layers over a silt-sized sediment bed in the laboratory, despite the fact that several authors call upon the need to test formulations for these environments under more realistic conditions [e.g., *Maa and Mehta*, 1987; *Traykovski et al.*, 2000; *Vinzon and Mehta*, 1998; *Winterwerp*, 2001]. Most laboratory studies that have produced turbulent wave boundary layers have done so in the absence of sediment that was fine enough to be easily suspended [e.g., *Hino et al.*, 1983; *Jensen et al.*, 1989]. Laboratory experiments that have used finer sediment

0148-0227/04/2004JC002355$09.00

Table 1. Sediment Experiments[a]

	Experiment														
	S1	S2	S3	S4	S5	S6	S7	S8	S9	S10	S11	S12	S13	S14	S15
U_{orb}, cm/s	21.7	23.8	28.3	30.3	31.9	37.2	41.1	30.6	33.5	44.6	55.0	52.3	40.6	38.0	38.2
T_w, s	5.97	7.67	5.85	4.29	7.55	5.90	7.54	6.12	4.94	4.90	5.65	4.22	5.95	4.97	4.28
C_{ave}, g/L	n/a	n/a	n/a	6.0	6.4	8.9	9.2	7.8	14.0	16.0	20.1	20.8	21.0	25.0	25.4
C_{bed}, g/L	3.2	7.1	10.7	17.3	20.5	22.3	24.7	29.1	33.8	47.0	50.1	53.3	50.8	73.9	80.7
H, cm	no HDS	no HDS	no HDS	7.80	7.34	6.83	7.17	7.05	5.11	3.13	3.78	3.88	3.33	4.72	4.65
$\overline{D_{50}}$, μm	n/a	n/a	n/a	21.20	33.63	25.01	34.43	34.33	35.81	66.32	36.57	48.35	60.75	59.05	61.61
η, cm	0.86	1.22	0.20	1.30	0.60	0.50	0.50	0.75	0.65	0.75	plane	1.10	0.43	0.68	0.75
δ_{bl}, cm	2.49	0.95	1.04	?	1.63	0.80	<0.3	<0.3	<0.3	<0.3	<0.3	<0.3	<0.3	<0.3	<0.3

[a]Measured values are from the 15 sediment experiments. The experiments were numbered from lowest to highest sediment concentration. Experiments S1–S3 did not produce definable high-density suspension (HDS). For experiments S7–S15, no boundary layers were measured. We assume that this was because the boundary layers were <3 mm in size, which was beyond the resolution of our instrumentation. Refer to the notation section for symbol definitions.

typically have used clay-sized sediment and examined small waves (i.e., wave heights <10 cm and wave periods <1 s) that did not produce fully turbulent boundary layers [e.g., *Maa and Mehta*, 1987]. In some investigations, waves were substituted by oscillatory shear in annular flumes [e.g., *Winterwerp and Kranenburg*, 1997], which has a different vertical profile of turbulence than well-developed wave boundary layers.

[4] More recently, M. P. Lamb and J. D. Parsons (High-density suspensions formed under waves, submitted to *Journal of Sedimentary Research*, 2004, hereinafter referred to as Lamb and Parsons, submitted manuscript, 2004) presented an experimental study on turbulent wave boundary layers over silt-dominated beds. They found that HDS formed over a wide range of wave conditions (Table 1). HDS had depth-averaged concentrations C_{ave} of 6–25 g/L, heights H of 2–8 cm, and depth-averaged mean grain sizes $\overline{D_{50}}$ of 21–62 μm (Table 1). HDS were separated from the upper water column by a lutocline (Figure 1). HDS formed after ~10 min of wave forcing, after which they did not significantly change concentration, grain size, or thickness for the duration of each experiment (~90 min), such that they were considered quasi-steady.

[5] In response to the need for laboratory data we performed a series of 15 freshwater experiments (F1–F15) and 15 sediment experiments (S1–S15) to characterize the wave boundary layer over an immobile false floor and over a silt-sized sediment bed, respectively. The sediment experiments presented here are the same experiments as those presented by Lamb and Parsons (submitted manuscript, 2004), which revealed the formation of HDS. Lamb and Parsons (submitted manuscript, 2004) presented measurements of the bed morphology and suspended sediment concentration and grain size inside HDS. Here we present new data on the vertical structure of velocity and turbulence inside HDS, which are used to construct a turbulent kinetic energy budget and to further elucidate the mechanics of high-density suspension formation. This data set will be compared to 15 new experiments (F1–F15) performed in the same facility under the same wave conditions but this time with no sediment.

2. Experimental Setup

[6] The experimental wave apparatus (Figure 2) is a sealed U tube capable of producing turbulent wave boundary layers under near-sinusoidal one-dimensional (1-D) horizontal oscillations with periods of 3–8 s and orbital velocities of 15–60 cm/s (Table 1). The U tube does not produce true orbital motions, which are typical under surface gravity waves near a free surface; rather, it produces one-dimensional, horizontally oscillating flow, which is typical of surface gravity wave motions near a fixed boundary (e.g., the seabed). For the freshwater experiments the Plexiglas false floor was roughened by fastening 120-grit sand paper (roughness ~0.1 mm), making the bottom boundary layer larger than the side boundary layers. For the sediment experiments the false floor was removed and replaced with a 10–15 cm thick sediment bed (silica flour) with a mean particle size of ~20 μm. The predominantly silt-sized mixture contained about 10% clay (D < 3.9 μm) and 20% sand (D > 63 μm). These wave and bed conditions are comparable to those observed during large storms in midshelf environments (e.g., Eel shelf [*Drake and Cacchione*, 1985; *Ogston et al.*, 2000; *Traykovski et al.*, 2000; *Wheatcroft and Borgeld*, 2000]). During an experiment, flow samples used for concentration and grain size measurements were taken with a rake of 11 vertically stacked siphons (Lamb and Parsons, submitted manuscript,

Figure 1. Photograph of the high-density suspension from experiment S9. The sediment was white. The lighting was from below and at an angle to maximize the visibility of the high-density suspension (HDS). Note the strong turbulent deformation in the suspension and the patchiness of the suspended sediment. The actual patchiness was greater than what appears in the photograph because of motion and smearing during the exposure time.

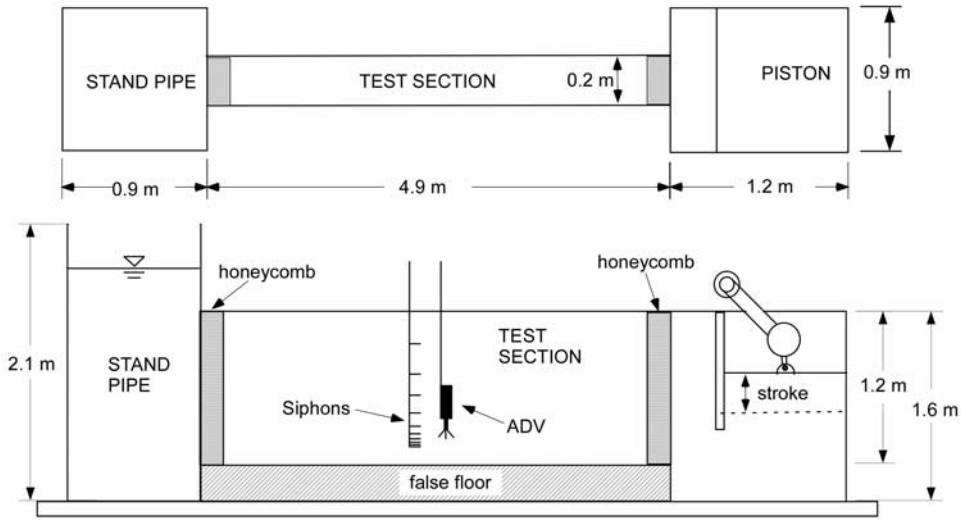

Figure 2. Schematic of experimental U tube in (top) plan view and (bottom) side view. The test section was completely sealed except for inlets into the two end tanks. The left end tank served as a standpipe with a free surface. In the right end tank a piston oscillated vertically, driving horizontal oscillations in the test section. Honeycomb between the end tanks and the test section minimized turbulent contamination in the test section from the end tanks. A rack of siphons and an acoustic Doppler velocimeter (ADV) were mounted near the center of the test section and were used to make flow measurements. The false floor was removed for the sediment experiments for placement of a sediment bed.

2004). Fifteen different orbital velocity-period combinations were used such that each freshwater experiment had a corresponding sediment experiment with nearly identical wave conditions (e.g., experiment F3 corresponds with S3 (Tables 1 and 2)).

[7] A micro–acoustic Doppler velocimeter (ADV) was mounted near the center of the test section (Figure 2). This instrument was used to measure the streamwise, cross-stream, and vertical components of velocity. The mount allowed the ADV to be adjusted vertically so that profiles of ~12 points in the vertical dimension were taken for each experiment. Each point was sampled at 50 Hz for ~5 min. The ADV has a small sampling volume (0.07 cm^3) and is able to make accurate measurements of velocity (±1%) and its vertical position from a solid boundary (±1 mm) when it is at least 3 mm away from the solid boundary. However, reliable velocity measurements are not possible when the sampling volume is closer than 3 mm from the bed. This is unfortunate since this region was often a significant portion of the wave boundary layer. A vertical scale on the ADV mount provided a second measure of the vertical position, which also had an error of ~1 mm based on repeated measurements. For the freshwater experiments both measures of vertical position were in good agreement. Unfortunately, the ADV was not able to detect its position with respect to the bed for the sediment experiments. The high concentrations of suspended sediment near the boundary likely obscured the peak in reflectance, making the distance to the boundary indeterminate. Therefore vertical elevations of the ADV above the bed were measured from the vertical scale on the ADV mount.

[8] Ripples commonly formed on the bed during the sediment experiments (Lamb and Parsons, submitted manuscript, 2004). While the position of the ADV had an absolute error of ~1 mm, locating the position of the bed with respect to the ADV proved more difficult because of the ripples. The position of the bed only could be located

Table 2. Freshwater Experiments[a]

	Experiment														
	F1	F2	F3	F4	F5	F6	F7	F8	F9	F10	F11	F12	F13	F14	F15
U_{orb}, cm/s	22.9	25.4	27.0	34.1	33.0	37.6	43.3	32.2	32.3	45.2	57.1	52.5	41.2	39.2	39.2
T_w, s	5.95	7.53	6.09	4.12	7.43	5.89	7.64	6.02	5.13	4.95	5.79	4.31	6.01	4.98	4.32
δ_{bl}, cm	0.99	1.31	1.18	0.96	1.38	1.24	1.64	1.18	1.13	1.56	1.18	1.10	1.39	1.13	1.02
δ_{gm}, cm	0.89	1.17	1.04	0.92	1.44	1.32	1.84	1.19	1.05	1.33	1.84	1.35	1.45	1.19	1.06
u_*, cm/s	0.40	0.69	0.60	0.68	0.89	0.85	1.21	0.83	0.78	1.32	1.48	1.34	1.11	1.03	1.00
u_{*gm}, cm/s	2.30	2.39	2.61	3.40	2.97	3.44	3.69	3.02	3.12	4.13	4.87	4.78	3.69	3.67	3.77

[a]Measured and computed values are from the 15 freshwater experiments. The experiments were numbered to correspond to the sediment experiments with the same wave conditions (U_{orb} and T_w). Refer to the notation section for symbol definitions. The modeled boundary layer height δ_{gm} was computed from $\kappa u_{*gm} T_w/2\pi$ for comparison with the measured boundary layer height δ_{bl}, where κ is Von Karman's constant (0.41). The bed shear velocity u_{*gm} was computed from the wave boundary layer model of *Grant and Madsen* [1979] using a roughness length of 1.5 mm (for best fit with δ_{bl}). An approximate near-bed shear velocity u_* was estimated as $(-\tau_A/\rho)^{1/2}$ from the points taken closest to the bed from each experiment for comparison with u_{*gm}; u_* was expected to be less than u_{*gm} because our measurements were still a significant distance above the constant stress portion of the boundary layer.

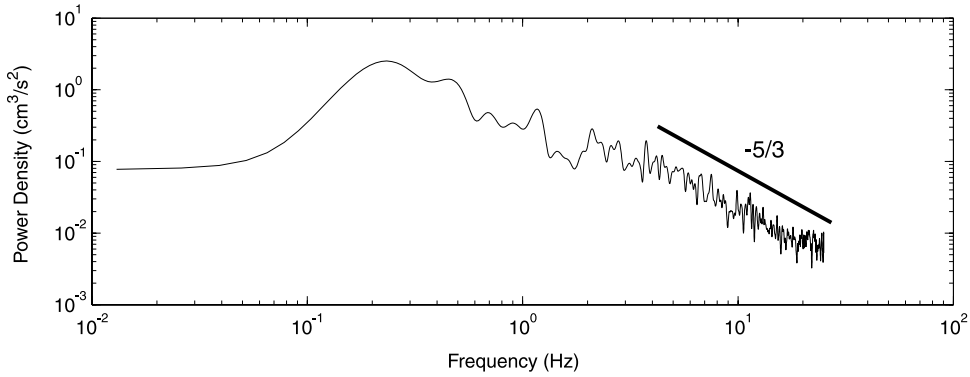

Figure 3. Spectrum of vertical velocity from experiment S15. The measurement was made 0.47 cm above the bed, a region where the highest sediment concentration from any of the experiments was measured (80.7 g/L). Note the −5/3 slope characteristic of the inertial subrange indicating turbulent flow. The vertical velocity spectrum was used for measurements of the turbulent dissipation rate to avoid contamination from the mean wave motions.

from visual estimates on the side of the U tube, but the ADV and siphons were located in the center of the U tube. The actual bed elevation underneath the instruments was assumed to be equivalent to the elevation of the bed at the side of the U tube where visual measurements were made. The average heights of the ripples for each experiment (Table 1) were used as an estimate of the vertical error.

3. Data Analysis

[9] Velocity data were collected using the ADV where each point in space consisted of a time series of velocity measurements in the x, y, and z directions; x is the streamwise dimension, y is the cross-stream dimension, and z is the vertical dimension, with positive being upward. The corresponding velocities in the x, y, and z directions are defined as u, v, and w, respectively. The ends of the time series data were cropped, so that each time series record contained complete wave cycles. Each velocity point is a function of its position in the vertical dimension and time t, or $\mathbf{u}(z, t)$.

3.1. Separating Waves and Turbulence

[10] Separating wave orbital motions from turbulent fluctuations is difficult when there is not a large spectral gap between the frequencies of the wave motions and the turbulent fluctuations (Figure 3). Some methods make use of an independent measure of orbital velocity by using a separate pressure sensor [*Pepper and Stone*, 2002] or velocity sensor [*Shaw and Trowbridge*, 2001; *Trowbridge*, 1998]. Such instrumentation was not available in these experiments. Consequently, the orbital motions were separated from the turbulent fluctuations using a tenth-order Butterworth filter with a cutoff frequency of 1.25 Hz (Figure 4). Similar techniques with a 1 Hz [*Foster et al.*, 2000] and a 2 Hz [*Smyth et al.*, 2002] cutoff frequency have been used. The total velocity $\mathbf{u}(z, t)$ was separated into the mean motions $\mathbf{U}(z, t)$ and the corresponding turbulent fluctuations $\mathbf{u}'(z, t)$, where $\mathbf{u}(z, t) = \mathbf{U}(z, t) + \mathbf{u}'(z, t)$.

3.2. Orbital Motions

[11] Once the turbulent fluctuations were removed from the data, several characteristic values of the orbital motion were calculated from the velocity time series. A vertically dependent maximum orbital velocity was calculated as $U_0(z) = \sqrt{2}U_{\mathrm{rms}}(z)$, where U_{rms} is the root-mean-square of U. The free stream maximum orbital velocity, herein referred to as the orbital velocity (U_{orb}), was defined as the vertical average of $U_0(z)$ for $z > 10$ cm, so that all points were in the free stream (i.e., not in the boundary layer). The wave period (T_w) was calculated as the average time between every other zero crossing in the velocity data.

3.3. Turbulent Motions

3.3.1. Turbulent Kinetic Energy

[12] The turbulent kinetic energy (TKE) was calculated for each point in the vertical dimension according to

$$\mathrm{TKE} = \frac{1}{2}\rho\left(\overline{u'^2} + \overline{v'^2} + \overline{w'^2}\right), \tag{1}$$

where the density of the fluid ρ was assumed to be equal to that of freshwater (1.0 g/cm^3), which is a reasonable

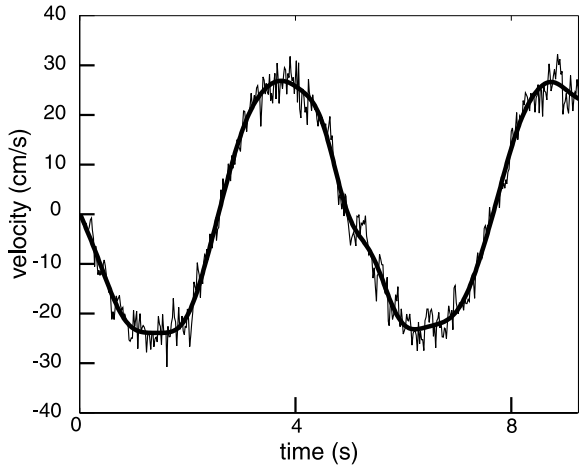

Figure 4. A section of velocity time series from experiment F9 at 0.4 cm above the bed inside of the boundary layer. The thin line shows the complete velocity series ($u = U + u'$). The thick line shows the orbital motions (U) after the turbulent fluctuations (u') have been removed using a 1.25 Hz cutoff frequency.

approximation since sediment concentrations of 80 g/L only increase the fluid density by ~5%. The overbars denote a temporal average.

3.3.2. Reynolds Stress and Turbulent Production

[13] The Reynolds stress τ is the measure of turbulent momentum flux or, equivalently, the shear stress due to turbulence. In steady 2-D boundary layer flow it is negative when given by $\tau = \rho\overline{u'w'}$, where u' is taken as positive downstream and w' is taken as positive upward [*Tennekes and Lumley*, 1972]. In an oscillatory boundary layer, U switches directions every half-wave cycle, such that quantity $u'w'$ also oscillates with the phase of the wave. Therefore, if $u'w'$ is averaged over all time in a symmetrically oscillating boundary layer, the result tends toward zero.

[14] It is ideal to calculate a Reynolds stress for each phase of the wave for an oscillatory boundary layer [*Hino et al.*, 1983; *Jensen et al.*, 1989]. Unfortunately, we were unable to make vertical profiles of phase-dependent Reynolds stresses with the instrumentation available because we lacked an independent measure of the phase. We calculated a characteristic Reynolds stress τ_A on the basis of a simple phase-averaging technique with only two bins: $0-\pi$ and $\pi-2\pi$. Instead of choosing a fixed positive x direction we defined the positive x direction at time t as the direction of the orbital motions $U(t)$ (e.g., Figure 4). Thus a positive turbulent fluctuation in the x dimension ($u' > 0$) at a specific height above the bed at a specific time was always a perturbation in the direction that the wave was moving at that height above the bed and at that time. Since oscillatory motions were confined to the x dimension, the y axis and z axis remained fixed. Once u' was redefined according to the changing x direction, the product $u'w'$ was calculated and time averaged over the entire time series. When multiplied by ρ, this product yielded a measure of the phase-averaged Reynolds stress τ_A. Though variability in τ occurs throughout the wave cycle, τ_A should serve to characterize the magnitude of the Reynolds stress for the entire wave. The phase-averaged production of TKE by shear was calculated at each point in the vertical by

$$P = -\tau_A \frac{dU_0}{dz}, \tag{2}$$

where the velocity gradient was obtained using a linear, centered, finite difference approximation.

3.3.3. Turbulent Dissipation Rate

[15] Within the inertial subrange the longitudinal spectrum of turbulent fluctuations $S_{11}(k)$ is a function of the turbulent dissipation rate ε given by [*Tennekes and Lumley*, 1972]

$$S_{11}(k) = a\varepsilon^{2/3}k^{-5/3}, \tag{3}$$

where k denotes wave number and $a = 0.5$ is the universal Kolmogorov constant [*Sreenivasan*, 1995]. In order to calculate the rate of dissipation from a time series it is necessary to convert from frequency space to wave number space. This conversion can be made by Taylor's hypothesis of frozen turbulence. Taylor's hypothesis supposes that

$$S_{ii}(k) = S_{ii}(f)/(2\pi/U_c), \tag{4}$$

where f denotes frequency and U_c denotes the mean velocity of a steady current. In an oscillating boundary layer it is unclear how to apply equation (4) directly because of the absence of a steady mean current. Through an asymptotic analysis, *Lumley and Terray* [1983] showed that when the wave orbital velocity is large compared to a superimposed mean current, the energy spectrum in both the longitudinal (subscript 1) and vertical (subscript 3) directions approaches

$$S_{11}(f) = S_{33}(f) \rightarrow \frac{7}{9}\Gamma\left(\frac{1}{3}\right)a\varepsilon^{2/3}U_{orb}^{2/3}(4\pi f)^{-5/3}, \tag{5}$$

where Γ denotes the gamma function. Equation (5) has been used to calculate the turbulent dissipation rate for the present experiments. Although the original derivation by *Lumley and Terray* [1983] was for near-surface wave orbits, which describe a circle, it has been used in marine bottom boundary layers where wave motions are horizontal [*Gross et al.*, 1994]. In order to minimize contamination of the turbulent spectrum from spectral leakage of the wave spectrum [e.g., see *Huntley and Hazen*, 1988] we used the spectra of the vertical fluctuations (e.g., Figure 3).

4. Review of Stratification Effects

[16] Before presenting data from this study it is useful to review some previous work on the effects of suspended sediment on a turbulent boundary layer. It has long been recognized that suspended sediment can affect the vertical structure of velocity and turbulence in unidirectional shear flows [*Einstein and Chien*, 1955; *Vanoni*, 1946]. Vertical mixing is damped, resulting in reduced diffusion of momentum, steepened near-bed velocity gradients, and a reduction in the size of the boundary layer [e.g., *Wang et al.*, 1998]. Many mechanisms have been proposed as causes for these observed effects including flocculation [*Wang et al.*, 1998], viscoelastic effects [*Li and Gust*, 2000], and decreased temporal spacing between turbulent bursts [*Best and Leeder*, 1993]. While there is debate about the mechanics of sediment-turbulence interactions, the observed changes in velocity profiles are often attributed to sediment-induced stratification [*Grant and Madsen*, 1986; *Winterwerp*, 2001].

[17] The effect of stratification can be expressed through a turbulent energy balance. Assuming horizontal homogeneity and a steady state, the local turbulent energy balance for a stratified fluid can be written as [*Turner*, 1973]

$$P + T = B + \varepsilon, \tag{6}$$

where T denotes the self-transport of turbulent energy (by pressure gradient work, velocity fluctuations, and viscous stresses) and B denotes the production of potential energy by work against the stable stratification. In turbulent boundary layers it is often assumed that T is negligible [*Turner*, 1973]. For cases with no density stratification, $B = 0$, and equation (6) reduces to the commonly used approximation $P = \varepsilon$.

[18] Perhaps the most common term used in describing stratified flow is a Richardson number [e.g., *Fernando*,

1991; *Hopfinger*, 1987]. One form of the Richardson number is the flux Richardson number Ri_f defined for shear flows as

$$Ri_f = \frac{B}{P}. \quad (7)$$

Theoretical considerations have shown that a critical value of Ri_f should exist ($Ri_{fc} \sim 0.15$), such that if $Ri_f > Ri_{fc}$, turbulence will collapse [*Turner*, 1973].

[19] It is extremely difficult to measure Ri_f because it requires simultaneous measurements of density and velocity with high temporal resolution. More often, the gradient Richardson number Ri_g has been used for stratified shear flows:

$$Ri_g = -\frac{g(\partial\rho/\partial z)}{\rho(\partial u/\partial z)^2}, \quad (8)$$

where g denotes acceleration due to gravity. *Howard* [1961] formulated a stability analysis on a two-dimensional, unidirectional flow in the presence of stratification. He found that for $Ri_g < 1/4$ the flow would be unstable with respect to the Kelvin-Helmholtz instability, which initiates mixing. Theoretical considerations have also shown that for $Ri_g > 1/4$, mixing is significantly damped because of the stratification [*Miles*, 1961].

[20] Several authors have used the concept of a critical Richardson number in analyzing oceanic currents with large amounts of suspended sediment. For example, *Wolanski et al.* [1992] measured sediment concentrations as high as 6 g/L in tidal currents in the Norbandy estuary, Australia, and created a model that emphasized sediment-induced anisotropic turbulence that limited vertical mixing. *Kineke et al.* [1996] used a Richardson-based closure model for suspensions on the tidally dominated Amazon shelf, which stressed the roles of vertical stratification and hindered settling. *Friedrichs et al.* [2000] showed that $Ri_g \sim 1/4$ in the bottom boundary layer of many coastal seas and bays with an abundant supply of easily suspendible fine sediment. Many oceanic bottom boundary layer models include the effects of stable stratification in unidirectional currents, though it is often neglected in the wave boundary layer [*Glenn and Grant*, 1987; *Styles and Glenn*, 2000].

5. Results

[21] Each experiment had a different wave orbital velocity and wave period combination (Table 1), which was dictated by the operational velocity-period combinations of the experimental apparatus (Lamb and Parsons, submitted manuscript, 2004). The sediment experiments are numbered (S1–S15) according to the near-bed concentration of sediment recorded during each experiment, with experiment S1 being the least concentrated. For each sediment experiment, there was a corresponding freshwater experiment with nearly the same wave orbital velocity and wave period (Table 2) in order to compare the boundary layers in the absence of sediment. The freshwater experiments are numbered (F1–F15) to correspond with their matching sediment experiment (e.g., F1 had the same wave conditions as S1).

5.1. Sediment Concentration Profiles

[22] As summarized in section 1 and described in detail by Lamb and Parsons (submitted manuscript, 2004), most of the sediment experiments (S4–S15) produced a concentrated layer of suspended sediment (Figure 5a), which became visible above the bed a few minutes after a run commenced (Figure 1) and did not change significantly in height or concentration for the duration of an experiment ($\sim$90 min). In general, experiments with higher wave orbital velocities had HDS with higher near-bed (C_{bed}) and depth-averaged (C_{ave}) sediment concentrations (Figure 6). Experiments S1–S3 did not produce definable lutoclines and had the lowest values of U_{orb} (<29 cm/s) and C_{bed} (<11 g/L).

5.2. Orbital Velocity Profiles

[23] For the freshwater experiments the vertical profiles of depth-dependent orbital velocity U_0 can be divided into three regions: the boundary layer, the overshoot, and the free stream (Figure 5b). We define the boundary layer as the closest portion of the flow to the bed, where $dU_0/dz > 0$. Above the boundary layer is the overshoot region, where U_0 exceeds U_{orb} and $dU_0/dz < 0$. Above the overshoot region is the free stream portion of the flow, where $U_0 \cong U_{\mathrm{orb}}$ and $dU_0/dz \cong 0$. The top of the boundary layer is defined as the elevation where the velocity gradient goes to zero, which is also the elevation where the velocity overshoot is at its maximum. For the freshwater experiments the boundary layer ranged in thickness from 1.0 to 1.7 cm (Table 2) in different experiments because of different wave orbital velocities and wave periods, but the forms of the velocity profiles were similar: boundary layer, overshoot, and free stream. The wave boundary layers in our freshwater experiments are consistent in vertical form to observations in nature [*Foster et al.*, 2000; *Trowbridge and Agrawal*, 1995], in the laboratory [*Hino et al.*, 1983; *Jensen et al.*, 1989], and in theory [*Batchelor*, 1967; *Grant and Madsen*, 1986]. Boundary layer heights calculated from the *Grant and Madsen* [1979] wave boundary layer model compare favorably with our measured values (Table 2).

[24] The velocity profiles from the sediment experiments do not exhibit the same vertical structure as the freshwater experiments (Figure 5b). For the experiments with lower sediment concentrations (S1–S3), there is some evidence for the three regions described in the freshwater experiments. However, with increasing sediment concentration, there is less evidence for a boundary layer and an overshoot region in the profiles. In fact, for experiments S5–S15, there was not a single measurement near the bed where $U_0 < U_{\mathrm{orb}}$.

5.3. Reynolds Stress Profiles

[25] The characteristic Reynolds stress τ_A was negative in the boundary layer for the freshwater experiments, which was expected as discussed in section 3 (Figure 5c). Since the sense of shear was opposite in the overshoot region from that in the boundary layer, it follows that the τ_A was positive in the overshoot region. In the free stream region, τ_A went to zero because the velocity profile had no shear.

[26] Like the velocity profiles, the vertical profiles of Reynolds stress in the presence of sediment were quite different from the freshwater profiles (Figure 5c). For the lower-concentration experiments (S1–S5) the Reynolds

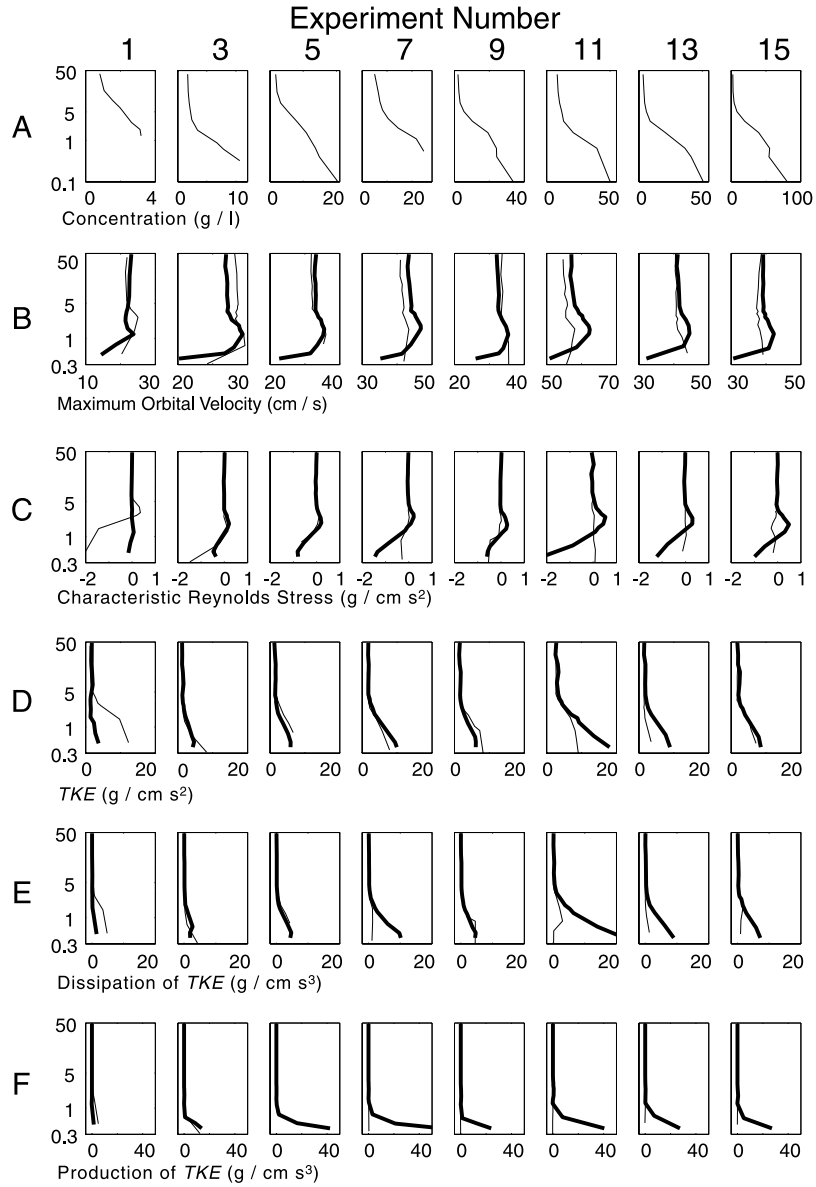

Figure 5. Semilog vertical profiles of (a) sediment concentration, (b) depth-dependent maximum orbital velocity, (c) characteristic Reynolds stress, (d) turbulent kinetic energy (TKE), (e) rate of dissipation of turbulent kinetic energy, and (f) rate of production of turbulent kinetic energy for the odd-numbered experiments. The thick lines correspond to the freshwater experiments, and the thin lines correspond to the sediment experiments. The vertical scales are logarithmic in centimeters above the bed. The horizontal scales are linear. Profiles from the even-numbered experiment are not shown to avoid redundancy. These even-numbered experiments follow the dominant trends in the profiles shown. The sediment experiments were numbered in order of increasing sediment concentration, with S15 being the most concentrated. The freshwater experiments were numbered to correspond with the sediment experiments that had nearly the same wave conditions (e.g., F1 corresponds to S1). Each sediment profile had vertical error on the order of the average ripple height given in Table 1. Note that the origins of the x axis for the plots of production and dissipation of turbulent kinetic energy are -5 and -2, respectively, not zero.

stress profiles were similar to those from the freshwater experiments where boundary layer, overshoot, and free stream regions were distinguished. However, with increasing sediment concentration, there was no boundary layer or overshoot region in the data. The Reynolds stress profiles for experiments S11–S15 indicate free stream flow throughout the measured water column. While the magnitude of τ_A increased with increasing orbital velocity for the freshwater experiments, this trend was not true for the sediment experiments. Instead, the dominant control on τ_A for the sediment experiments was an inverse relationship with the concentration of suspended sediment.

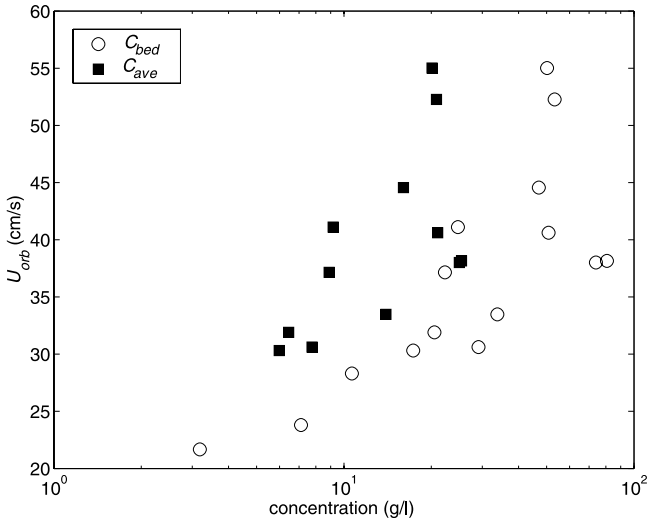

Figure 6. Near-bed sediment concentration (C_{bed}) and depth-averaged sediment concentration within the HDS (C_{ave}) versus orbital velocity (U_{orb}) for all of the sediment experiments.

[27] The near-bed values of τ_A for the freshwater experiments correlate well with predictions of bed stress from wave boundary layer models [*Grant and Madsen*, 1979; *Swart*, 1974] (Table 2). This lends support for our use of a phase-averaged Reynolds stress. While the magnitude of our near-bed τ_A was less than predicted from the models, our near-bed measurements were >3 mm above the bed, which was >30% of the boundary layer thickness, placing them well outside of the constant stress layer where such a comparison is applicable [*Tennekes and Lumley*, 1972].

[28] The vertical structure of Reynolds stress in the wave boundary layer has an important implication in defining the top of the boundary layer from laboratory or field data. From the velocity profile it is difficult to identify the top of the wave boundary layer because this value must be extrapolated between data points without knowing the vertical structure. An alternative method is to recognize that the top of the wave boundary layer is the location where the velocity overshoot reaches its maximum, such that $\tau_A = 0$. Identifying the zero crossing in the Reynolds stress profile provides a simple estimate of the boundary layer thickness δ_{bl}, which was done for our experiments using a linear interpolation between data points (Tables 1 and 2).

5.4. Turbulent Kinetic Energy Profiles

[29] Both the sediment and the freshwater experiments had similar vertical profiles of TKE (Figure 5d). TKE was small in the upper water column and increased near the bed. There was a slight level of background TKE in all of the experiments evidenced by the constant values of TKE in the free stream region. This was likely generated in the end tanks and advected or diffused horizontally into the test section. Although we intentionally tried to minimize background TKE with the experimental design (Figure 2), we expect that small levels of background turbulence should not pose an analog problem with nature because background turbulence is common in marine environments (see discussion by Lamb and Parsons (submitted manuscript, 2004)). For both the freshwater and the sediment experiments, TKE was not confined to the boundary layer, as is often assumed. For the freshwater experiments the flow had enhanced levels of TKE (above background levels) to elevations ~5 cm above the bed, significantly higher than the top of the boundary layer (Table 2). The sediment experiments also had enhanced levels of TKE at elevations ~5 cm above the bed, even when no boundary layer was detected (e.g., S11 in Figure 5d).

[30] For the freshwater experiments the magnitude of TKE increased with increasing orbital velocity, while for the sediment experiments this trend was not clear (Figure 7). There was no clear damping of TKE in the sediment experiments when compared to their corresponding freshwater experiments. In general, all of the sediment experiments had approximately equal levels of TKE despite differences in orbital velocity and sediment concentration, although there was significant scatter. Note that in the absence of suspended sediment the TKE for the sediment experiments would likely have been higher than the freshwater experiments because of increased drag due to ripples on the bed. This can be seen by comparing the sediment experiments with the lowest orbital velocity (and lowest suspended sediment concentration (Figure 6)) with their corresponding freshwater experiments (Figure 7).

5.5. Production and Dissipation Profiles

[31] The vertical profiles of turbulent dissipation rate ε roughly followed the form of the vertical profiles of TKE for both the sediment and the freshwater experiments, since regions that had turbulent energy should also be regions where turbulent energy was dissipating (Figure 5e). Like TKE, the profiles of ε show evidence that there was

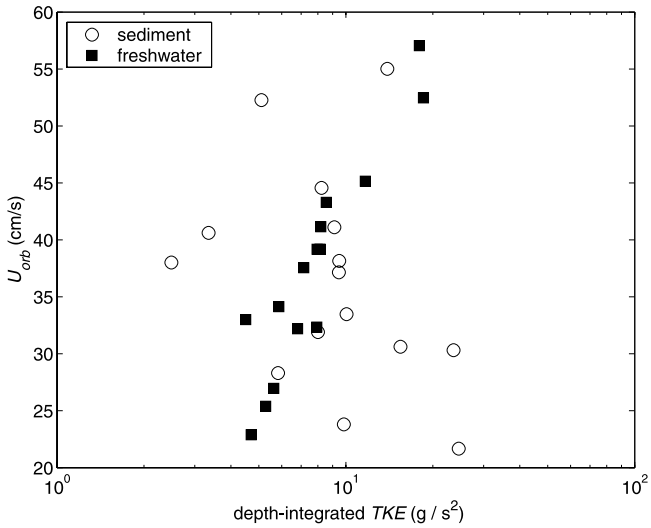

Figure 7. Depth-integrated turbulent kinetic energy versus orbital velocity (U_{orb}) for all of the experiments. The background TKE, assumed to be the vertical average of the free stream TKE (z > 10 cm), was depth integrated and subtracted from the values shown.

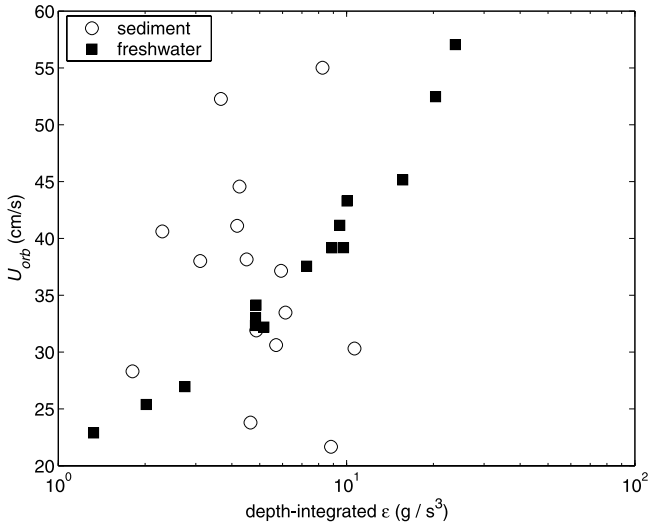

Figure 8. Depth-integrated turbulent dissipation rate versus orbital velocity (U_{orb}) for all of the experiments. The background ε, assumed to be the vertical average of the free stream ε (z > 10 cm), was depth integrated and subtracted from the values shown.

enhanced turbulence above the wave boundary layer in both the sediment and the freshwater experiments. For the freshwater experiments, ε increased with increasing orbital velocity, while the sediment experiments did not follow this trend (Figure 8).

[32] The profiles of turbulent energy production P were significantly different from ε and TKE for the freshwater experiments (Figure 5f). Turbulent production was greatest in the boundary layer region because this was a region with both significant velocity gradients and Reynolds stresses (equation (2)). For the freshwater experiments, P was high very near the bed in the boundary layer and decreased sharply to a value near zero slightly below the top of the boundary layer. As a result, P did not equal ε; P dominated over ε in the lower part of the boundary layer, while ε dominated over P in the upper portion of the boundary layer and in the upper water column.

[33] For the sediment experiments the profiles of P were much different from the freshwater experiments (Figure 5f). For the lower-concentration experiments, there was some P near the bed (S1–S3). However, with increasing sediment concentration, P rapidly went to zero. This led to a large discrepancy between P and ε; that is, $P \neq \varepsilon$. The vertically integrated values of P for the sediment experiments were reduced significantly from their freshwater counterparts as orbital velocity and sediment concentration increased (Figure 9).

6. Discussion

6.1. Problems With ADV

[34] All of the ADV data obtained in these experiments had signal-to-noise ratios (>50 dB) and correlations (>90%) within the limits of accurate data according to the manufacturer (SonTek, personal communication, 2003). However, it might be possible that miscalculations within the ADV software caused the observed boundary layer changes because the ADV was not designed for measurements in such highly concentrated suspensions. For example, the upper section of the sampling volume might be favored over the lower section because the sediment in suspension would give abundant acoustic reflectors for the upper part while scattering and dissipating the returns from the lower part. However, this does not appear to be the case because *Gratiot et al.* [2000] showed that the ADV was not significantly affected by concentrations as high as 100 g/L. Therefore, while the sediment did not allow the ADV to detect the boundary, we will assume that the ADV still gave accurate velocity measurements in the HDS.

6.2. Boundary Layer Reduction

[35] It is clear from the data that the boundary layer was not observed for experiments with high near-bed sediment concentrations (>20 g/L) as shown in the vertical profiles of velocity, Reynolds stress, and turbulent production. We suspect that sediment-induced stratification resulted in less efficient mixing of momentum near the bed and therefore a reduction in the size of the boundary layer. This hypothesis is partially supported by the reduced boundary layer size with increasing sediment concentration for the lower-concentration sediment experiments (S1–S6), although there is significant scatter (Table 1). For the sediment experiments with no observed boundary layer (S7–S15) the boundary layer must have been reduced to a size <3 mm (Table 1). Measuring velocities within 3 mm of the bed is beyond the capabilities of the ADV. The boundary layers were reduced in size substantially because all of the freshwater experiments with the same wave conditions had boundary layers >1 cm (Table 2). It is important to note that under nonstratified conditions the boundary layers in the sediment experiments likely would have been larger than the

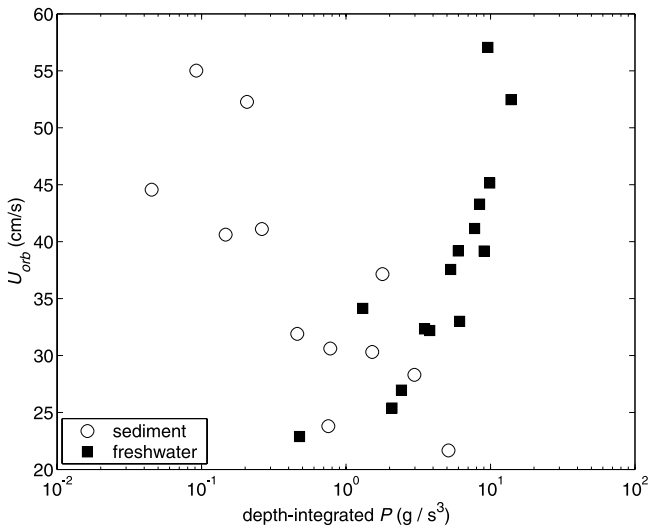

Figure 9. Depth-integrated turbulent production rate versus orbital velocity (U_{orb}) for all of the experiments. The background P, assumed to be the vertical average of the free stream P (z > 10 cm), was depth integrated and subtracted from the values shown.

freshwater experiments because of the roughness imposed by ripples on the bed.

[36] Our finding of boundary layer reduction is significant because, as described in section 1, while an increase in near-bed velocity gradients and/or boundary layer reduction has been recognized in steady unidirectional flows, to our knowledge it has not been observed previously in wave boundary layers. Furthermore, stratification effects are often neglected in wave boundary layer models, even when they are accounted for in unidirectional boundary layer models [*Glenn and Grant*, 1987; *Styles and Glenn*, 2000]. In addition, boundary layer reduction of this magnitude (approximately an order of magnitude) has not been observed in unidirectional flows. This might be due to the fact that steady currents have sufficient time to develop boundary layers, even in the presence of stratification. Reduced momentum transfer not only reduces the size of a boundary layer but also likely increases the time needed to develop a boundary layer. The boundary layers in our experiments only had $\sim(1/2)T_w$ (i.e., 1.5–4 s) to develop, making boundary layer reduction significant.

6.3. Turbulence in High-Density Suspensions

[37] Despite the high sediment concentrations and reduced thickness of the wave boundary layer the water column within and significantly above the δ_{bl} was turbulent. It is often assumed that significant turbulent energy is only available within the boundary layer region since it is the region of production of TKE by shear and that high concentrations of sediment will significantly damp turbulence. Our profiles of TKE and ε clearly show that the water column had enhanced levels of turbulence (above background values) within the HDS and at elevations much greater than δ_{bl} (Figure 5). In addition, velocity power spectrums exhibited a $-5/3$ dependence on frequency, which is characteristic of the inertial subrange for turbulent flow [*Tennekes and Lumley*, 1972]. The $-5/3$ slope was prevalent in all of the data taken inside HDS, even for experiment S15 at 0.47 cm above the bed (Figure 3), which was the region of highest measured sediment concentration (80.7 g/L) in all of our experiments. This turbulence supported HDS of silt-sized particles to elevations significantly above the top of the boundary layer (Table 1).

6.4. Turbulent Kinetic Energy Budget

[38] Since the HDS were turbulent but no local production of turbulence was observed at high sediment concentrations (Figure 5e), the turbulent energy that we measured in the water column must have been transported into the region where the sediment was suspended. Consider the importance of the transport of turbulent energy for the freshwater experiments. For flows with no stratification ($B = 0$) the turbulent energy balance shown in equation (6) reduces to

$$P + T = \varepsilon. \tag{9}$$

If turbulent transport is neglected, equation (9) reduces to the familiar expression $P = \varepsilon$. As shown in the profiles for the freshwater experiments, this was clearly not the case (Figure 5). Dissipation was consistently greater than production in the overshoot region and in the top portion of the boundary layer. However, near the bed, production dominated over dissipation. Thus T is likely to be of first-order importance for wave boundary layers.

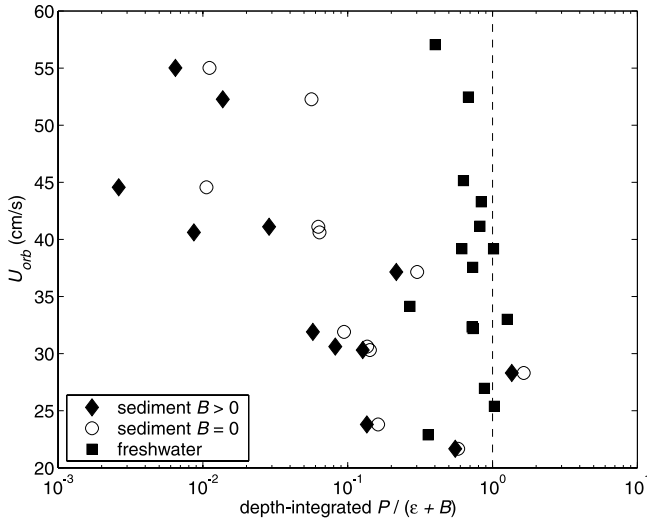

Figure 10. Depth-integrated rates of turbulent production divided by turbulent dissipation plus buoyancy production versus orbital velocity (U_{orb}) for all of the sediment and freshwater experiments. $B = 0$ for the freshwater experiments. For the sediment experiments with $B > 0$, B was estimated from equation (11). The sediment experiments are also shown with $B = 0$ to demonstrate that the inequality shown for the sediment experiments was not a result of B.

[39] Unfortunately, we were not able to measure T directly in our experiments because of our instrumentation. However, by recognizing that T integrated over the domain is equal to zero we constructed a depth-integrated turbulent energy balance for the sediment experiments. Integrating equation (9) over our measurement domain yields

$$\int_{0.3\mathrm{cm}}^{50\mathrm{cm}} P dz = \int_{0.3\mathrm{cm}}^{50\mathrm{cm}} \varepsilon dz. \tag{10}$$

As shown in Figure 10, equation (10) was reasonably satisfied for the freshwater experiments.

[40] We now construct the same energy balance for the sediment experiments, but this time we must include B. Unfortunately, we also were not able to measure B directly because B involves fluctuating quantities of both velocity and sediment concentration. In quasi-steady suspensions, such as in these experiments, it is common to equate the buoyancy flux B with a settling flux [e.g., *Huppert et al.*, 1995; *Winterwerp*, 2001]:

$$B \equiv Rg\overline{w'c'} = Rgw_s c, \tag{11}$$

where c denotes the dimensionless volumetric sediment concentration, c' denotes the temporal fluctuating component of c, and R denotes the relative excess density of the sediment ($R = (\rho_s - \rho_w)/\rho_w$, where ρ_s denotes the density of

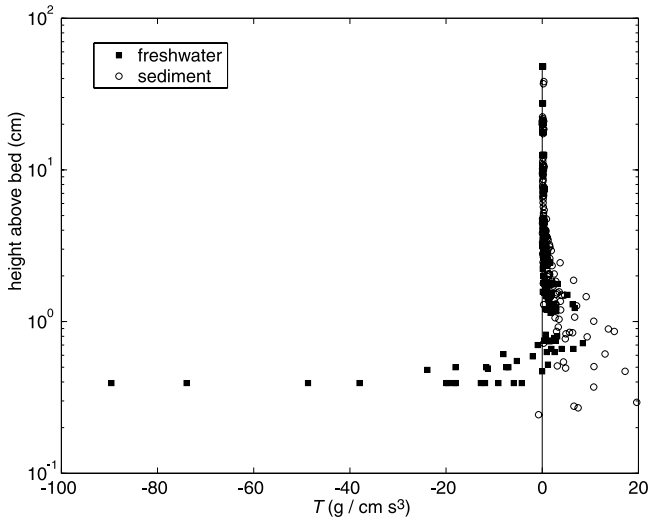

Figure 11. Vertical profile of the rate of transport of TKE (T) for all of the experiments, calculated from equations (6) and (9) for the freshwater and sediment experiments, respectively. Negative values of T indicate that energy was transported out of the region. Positive values of T indicate that energy was transported into the region.

sediment and ρ_w denotes the density of water), which was ~1.65 for our experiments. The settling velocity w_s was calculated using Stokes' law and D_{50}. Integrating equation (6) and assuming that $\int_{0.3\text{cm}}^{50\text{cm}} Tdz = 0$ yields

$$\int_{0.3\text{cm}}^{50\text{cm}} Pdz = \int_{0.3\text{cm}}^{50\text{cm}} \varepsilon dz + \int_{0.3\text{cm}}^{50\text{cm}} Bdz. \qquad (12)$$

For our sediment experiments this equality was not satisfied (Figure 10), especially at high sediment concentrations (Figure 6). Setting $B = 0$ in equation (12) reveals that the inequality was not due to an overestimate of the buoyancy term (Figure 10). As long as B was nonnegative, which was almost certainly true because of the stable stratification, the inequality in the sediment experiments implies that $\int_{3\text{mm}}^{50\text{cm}} Tdz \neq 0$. The vertical integration neglected the lower 3 mm of the water column, which was a region that encompassed a significant portion of the boundary layer or the entire boundary layer at high sediment concentrations. Since the boundary layer was likely a region where P dominated over ε (on the basis of the freshwater experiments (Figure 5)), this integration neglected a significant portion of the TKE budget. The strong deviation of P/ε to a value much less than unity indicates that increasing amounts of turbulent energy production were occurring within 3 mm of the bed with increasing sediment concentration, which is consistent with the boundary layer reduction hypothesis.

[41] While we were not able to measure T independently, we did calculate it using equation (6) for the sediment experiments and equation (9) for the freshwater experiments (Figure 11). For the freshwater experiments the negative values of T near the bed indicate that turbulent energy was being transported out of this region. These negative values of T were compensated by energy being transported into the system above, such that energy was conserved. Note that the magnitude of T was of the same order as ε, making it of first-order importance. The sediment experiments were much different. The rates of energy transport into the upper fluid region were even greater than in the freshwater experiments. However, there were no calculated negative values of T to compensate for this energy sink. This transported energy must have been produced in the very thin region near the bed that we were unable to measure in order to conserve energy.

6.5. Richardson Number

[42] As discussed in section 4, the degree of turbulence reduction is often assessed through the use of a Richardson number. Both a flux Richardson number Ri_f and a gradient Richardson number Ri_g (as defined in equations (7) and (8), respectively) were calculated at each point in the vertical dimension for each sediment experiment (Figure 12). The concentration and velocity gradients were calculated using a centered linear finite difference approximation. None of the experiments show Ri_g or Ri_f maintaining a critical or constant value in the vertical direction. In fact, except for a few points, all values of Ri_g and Ri_f are significantly greater than their assumed critical values of ~1/4.

[43] These values of Ri_g and Ri_f do not make sense because our observations and measurements indicated that the HDS were turbulent and sediment was held in suspension. For $Ri_g \gg Ri_{gc}$ or $Ri_f \gg Ri_{fc}$, turbulence should be completely damped [*Turner*, 1973], which would result in sediment settling. A value near 1/4 is expected for our experiments with HDS because they appeared to be held in a quasi-steady state through a feedback between suspended sediment and turbulence (Lamb and Parsons, submitted manuscript, 2004).

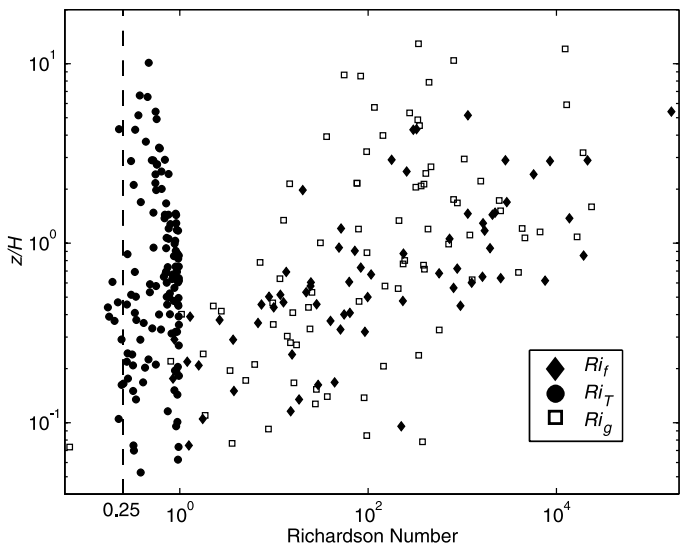

Figure 12. Vertical profile of the gradient Richardson number Ri_g, the flux Richardson number Ri_f for shear flows, and a flux Richardson number that includes T for shear-free flows Ri_T. All of the sediment experiments were combined, and the vertical scale was normalized by the height of the HDS from each experiment H.

[44] The discrepancy between the calculated and assumed critical values of Ri_g and Ri_f likely arose because the formulations used for Ri_g and Ri_f are applicable for stratified shear flows where turbulence is locally produced by the Kelvin-Helmholtz instability. We hypothesize that in some ways the HDS in our experiments behaved as shear-free flows. The source of the turbulence supporting the suspension was not local production but transported turbulence. The importance of T has been widely recognized in shear-free experiments where turbulence was generated from oscillating grids and transported or diffused into the region of interest [*Turner*, 1973]. When formulating a flux Richardson number for shear-free flows, T must be included as a source of turbulent energy [*Fernando*, 1991; *Hopfinger*, 1987]:

$$Ri_T = \frac{B}{P+T}. \tag{13}$$

As shown in Figure 12, the values of Ri_T are more reasonable. Note that for our experiments, Ri_T was necessarily held to a value between zero and unity because we did not independently measure T.

6.6. Model Summary

[45] To summarize, in sediment-free wave boundary layers, T was shown to be of first-order importance. More energy was produced than dissipated in most of the lower boundary layer (Figure 13). In the upper portion of the boundary layer and above the boundary layer, more energy was dissipated than was produced. The transport of energy allowed the water column to have enhanced turbulence at elevations 2–4 times greater than the boundary layer thickness.

[46] For sediment-stratified wave boundary layers, inefficient momentum transfer caused by sediment-induced stratification substantially reduced the size of the boundary layer (Figure 13). For experiments with near-bed concentrations greater than ~20 g/L the boundary layer was reduced to <3 mm. However, the water column above the boundary layer remained approximately as turbulent as in the freshwater experiments. In many cases the rates of turbulent energy being transported into the upper water column were as great as or greater than the rates calculated at the same elevations for the freshwater experiments (Figure 11). If the sediment experiments were producing approximately as much turbulent energy as the freshwater experiments, the production rates must have been large in the thin region near the bed (Figure 13). This seems plausible because the near-bed velocity gradients for the sediment experiments were likely much larger than the freshwater experiments. Thus stratification did not damp the turbulence in the bulk of the flow; rather, stratification changed the distribution of P and ε in the water column.

[47] The mechanism that transported the turbulent energy into the HDS remains unclear. This energy was transported along with suspended sediment from the near-bed region higher in the water column in a manner that prevented significant mixing of momentum and thickening of the boundary layer. One mechanism for transferring this energy might have been large but infrequent ejections. We visually observed vigorous ejections transporting sediment-rich fluid from the bed in to the upper portions of the HDS. These ejections were often coincident with the lee side of ripples. However, ripples were not a necessary condition for formation of HDS because experiment S11 produced a plane rather than a rippled bed. *Baas and Best* [2002] also noted an increase in the magnitude and a decrease in the temporal spacing of ejections in experiments on sediment-laden unidirectional currents when the concentration exceeded ~50 g/L. It is important to reaffirm that the mechanism that transported the turbulent energy might not have been related to the suspended sediment or the ripples since T was also of first-order importance in the freshwater experiments.

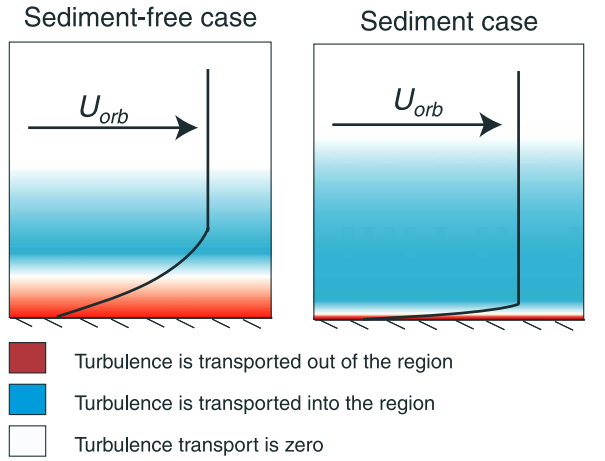

Figure 13. Idealized schematic of a wave boundary layer and its associated transport of turbulent energy T with and without sediment stratification. For the sediment-free case the boundary layer is on the order of centimeters thick. There is an excess of turbulent energy production compared to dissipation in most of the lower boundary layer. The upper portion of the boundary layer and the water column above the boundary layer possessed an excess of dissipation of TKE. T allows the flow to be turbulent well above the boundary layer. For the sediment case the boundary layer is only a few millimeters thick because of inefficient mixing of momentum caused by sediment-induced stratification. However, the water column is not less turbulent. Increased near-bed velocity gradients create a region of intense turbulent production very near the bed, and this energy is transported into the upper water column where it supports suspensions much thicker than the wave boundary layer in the absence of local shear.

6.7. Temporal Variability

[48] In our analysis we have purposely neglected time-dependent terms in the turbulent energy balance (equation (6)). Since our measurements were averaged over many wave periods and the wave forcing and suspended sediment concentration remained quasi-steady for the duration of an experiment, these time-dependent terms are likely not important for our calculations. However, our visual observations indicated that fluctuations in the turbulent structure and fluctuations in sediment concentration (e.g., from ejections) were common within a single wave period. For these processes the time-dependent energy terms would play a crucial role. For example, numerical models on stratified unidirectional flows have documented a collapse

of turbulence when either the turbulence or the concentration is perturbed [*Winterwerp*, 2001]. On intrawave timescales in our experiments the level of turbulence was constantly being perturbed because of the oscillatory wave forcing. Such a collapse might explain the lutoclines in these experiments. In addition, particle-turbulence interactions have been shown to lead to a gravitational collapse of patches of fluid and sediment [*McCool and Parsons*, 2004], which is consistent with our visual observations of the formation and destruction of concentrated sediment-fluid plumes inside HDS on these timescales (note the patchiness of sediment in Figure 1) (Lamb and Parsons, submitted manuscript, 2004).

7. Conclusions

[49] We report on a series of laboratory experiments of turbulent wave boundary layers over a predominantly silt-sized sediment bed. Detailed data on the vertical structure of turbulence and velocity show that suspended sediment greatly reduced the size of the wave boundary layer, oftentimes to <3 mm. However, turbulence was not confined to the wave boundary layer but was transported much higher into the water column. There it was able to support large concentrations of sediment as high as 8 cm above the bed. Boundary layer reduction and the transport of TKE must be taken into account when formulating Richardson-type models for HDS, or orders of magnitude errors could occur.

Notation

B rate of production of buoyant energy.
c volumetric concentration.
C_{ave} depth-averaged concentration within a high-density suspension.
C_{bed} concentration from sample taken nearest the bed.
D_{50} grain diameter which 50% of the mass distribution is finer than.
$\overline{D_{50}}$ depth-averaged D_{50} within a high-density suspension.
δ_{bl} measured boundary layer thickness.
δ_{gm} calculated boundary layer thickness from *Grant and Madsen* [1979].
ε rate of dissipation of turbulent kinetic energy.
HDS high-density suspension.
H height of HDS.
η ripple height.
P rate of production of turbulent kinetic energy.
R relative excess density of the sediment (1.65).
Ri_g gradient Richardson number.
Ri_{gc} critical gradient Richardson number.
Ri_f flux Richardson number.
Ri_{fc} critical flux Richardson number.
Ri_T flux Richardson number including T.
T self-transport of turbulent kinetic energy.
T_w wave period.
TKE turbulent kinetic energy.
τ_A characteristic Reynolds stress.
U_0 maximum depth-dependent orbital velocity.
U_{orb} maximum orbital velocity.
u streamwise velocity including mean motions and turbulent fluctuations.
u' fluctuating component of streamwise velocity.
u_* near-bed shear velocity calculated from τ_A closest to the bed.
u_{*gm} bed shear velocity calculated from *Grant and Madsen* [1979].
w_s setting velocity of sediment using Stokes' law and D_{50}.

[50] **Acknowledgments.** Financial support was kindly provided by the National Science Foundation (EAR-0309887), the Office of Naval Research (N000140310138), and the University of Washington. M.P.L. was funded by a National Defense Science and Engineering Graduate Fellowship. Rex Johnson and Randy Fabro built and helped design the U tube and provided invaluable assistance before and during the experiments. We thank Mike Gregg, Jim Riley, Mark Stacey, and two anonymous reviewers for helpful comments that clarified many of the topics presented in this paper.

References

Baas, J. H., and J. L. Best (2002), Turbulence modulation in clay-rich sediment-laden flows and some implications for sediment deposition, *J. Sediment. Res.*, *72*(3), 336–340.
Batchelor, G. K. (1967), *An Introduction to Fluid Dynamics*, 615 pp., Cambridge Univ. Press, New York.
Best, J. L., and M. Leeder (1993), Drag reduction in turbulent muddy seawater flows and some sedimentary consequences, *Sedimentology*, *40*, 1129–1137.
Drake, D. E., and D. A. Cacchione (1985), Seasonal variation in sediment transport on the Russian River shelf, California, *Cont. Shelf Res.*, *4*(5), 495–514.
Einstein, H. A., and N. Chien (1955), Effects of heavy sediment concentration near the bed on velocity and sediment distribution, *Mo. River Div. Sediment Ser. Rep. 8*, Univ. of California, Berkeley, Calif.
Fernando, H. J. S. (1991), Turbulent mixing in stratified fluids, *Annu. Rev. Fluid Mech.*, *23*, 455–493.
Foster, D. L., R. A. Beach, and R. A. Holman (2000), Field observations of the wave bottom boundary layer, *J. Geophys. Res.*, *105*(C8), 19,631–19,647.
Friedrichs, C. T., L. D. Wright, D. A. Hepworth, and S. C. Kim (2000), Bottom-boundary-layer processes associated with fine sediment accumulation in coastal seas and bays, *Cont. Shelf Res.*, *20*(7), 807–841.
Glenn, S. M., and W. D. Grant (1987), A suspended sediment stratification correction for combined wave and current flows, *J. Geophys. Res.*, *92*(C8), 8244–8264.
Grant, W. D., and O. S. Madsen (1979), Combined wave and current interaction with a rough bottom, *J. Geophys. Res.*, *84*(C4), 1797–1808.
Grant, W. D., and O. S. Madsen (1986), The continental-shelf bottom boundary-layer, *Annu. Rev. Fluid Mech.*, *18*, 265–305.
Gratiot, N., M. Mory, and D. Auchere (2000), An acoustic doppler velocimeter (ADV) for the characterization of turbulence in concentrated fluid mud, *Cont. Shelf Res.*, *20*(12–13), 1551–1567.
Gross, T. F., A. J. Williams, and E. A. Terray (1994), Bottom boundary-layer spectral dissipation estimates in the presence of wave motions, *Cont. Shelf Res.*, *14*(10–11), 1239–1256.
Hino, M., M. Kashiwayanagi, A. Nakayama, and T. Hara (1983), Experiments on the turbulence statistics and the structure of a reciprocating oscillatory flow, *J. Fluid Mech.*, *131*, 363–400.
Hopfinger, E. J. (1987), Turbulence in stratified fluids: A review, *J. Geophys. Res.*, *92*(C5), 5287–5303.
Howard, L. N. (1961), Note on a paper of John W. Miles, *J. Fluid Mech.*, *13*, 158–160.
Huntley, D. A., and D. G. Hazen (1988), Seabed stresses in combined wave and steady flow conditions on the Nova-Scotia continental-shelf—Field-measurements and predictions, *J. Phys. Oceanogr.*, *18*(2), 347–362.
Huppert, H. E., J. S. Turner, and M. A. Hallworth (1995), Sedimentation and entrainment in dense layers of suspended particles stirred by an oscillating-grid, *J. Fluid Mech.*, *289*, 263–293.
Jensen, B. L., B. M. Sumer, and J. Fredsoe (1989), Turbulent oscillatory boundary-layers at high Reynolds-numbers, *J. Fluid Mech.*, *206*, 265–297.
Kineke, G. C., R. W. Sternberg, J. H. Trowbridge, and W. R. Geyer (1996), Fluid-mud processes on the Amazon continental shelf, *Cont. Shelf Res.*, *16*(5–6), 667–696.
Li, M. Z., and G. Gust (2000), Boundary layer dynamics and drag reduction in flows of high cohesive sediment suspensions, *Sedimentology*, *47*, 71–86.

Lumley, J. L., and E. A. Terray (1983), Kinematics of turbulence convected by a random wave field, *J. Phys. Oceanogr.*, *13*(11), 2000–2007.

Maa, P. Y., and A. J. Mehta (1987), Mud erosion by waves—A laboratory study, *Cont. Shelf Res.*, *7*(11–12), 1269–1284.

McCool, W., and J. D. Parsons (2004), Sedimentation from buoyant fine-grained suspensions, *Cont. Shelf Res.*, *24*, 1129–1142 doi:10.1016/j.csr.2004.03.009.

Miles, J. W. (1961), On the stability of heterogeneous shear flow, *J. Fluid Mech.*, *10*, 496–508.

Ogston, A. S., D. A. Cacchione, R. W. Sternberg, and G. C. Kineke (2000), Observations of storm and river flood-driven sediment transport on the northern California continental shelf, *Cont. Shelf Res.*, *20*(16), 2141–2162.

Pepper, D. A., and G. W. Stone (2002), Atmospheric forcing of fine-sand transport on a low-energy inner shelf: South-central Louisiana, USA, *Geo Mar. Lett.*, *22*(1), 33–41.

Shaw, W. J., and J. H. Trowbridge (2001), The direct estimation of near-bottom turbulent fluxes in the presence of energetic wave motions, *J. Atmos. Oceanic Technol.*, *18*(9), 1540–1557.

Smyth, C., A. E. Hay, and L. Zedel (2002), Coherent Doppler profiler measurements of near-bed suspended sediment fluxes and the influence of bed forms, *J. Geophys. Res.*, *107*(C8), 3105, doi:10.1029/2000JC000760.

Sreenivasan, K. R. (1995), On the universality of the Kolmogorov constant, *Phys. Fluids*, *7*(11), 2778–2784.

Styles, R., and S. M. Glenn (2000), Modeling stratified wave and current bottom boundary layers on the continental shelf, *J. Geophys. Res.*, *105*(C10), 24,119–24,139.

Swart, D. H. (1974), Offshore sediment transport and equilibrium beach profiles, *Publ. 131*, Delft Hydraul. Lab., Delft, Netherlands.

Tennekes, H., and J. L. Lumley (1972), *A First Course in Turbulence*, 300 pp., MIT Press, Cambridge, Mass.

Traykovski, P., W. R. Geyer, J. D. Irish, and J. F. Lynch (2000), The role of wave-induced density-driven fluid mud flows for cross-shelf transport on the Eel River continental shelf, *Cont. Shelf Res.*, *20*(16), 2113–2140.

Trowbridge, J. H. (1998), On a technique for measurement of turbulent shear stress in the presence of surface waves, *J. Atmos. Oceanic Technol.*, *15*, 290–298.

Trowbridge, J. H., and Y. C. Agrawal (1995), Glimpses of a wave boundary layer, *J. Geophys. Res.*, *100*(C10), 20,729–20,743.

Turner, J. S. (1973), *Buoyancy Effects in Fluids*, 368 pp., Cambridge Univ. Press, New York.

Vanoni, V. A. (1946), Transportation of suspended sediment by water, *Trans. Am. Soc. Civ. Eng.*, *111*, 67–133.

Vinzon, S. B., and A. J. Mehta (1998), Mechanism for formation of lutoclines by waves, *J. Waterw. Port Coastal Ocean Eng.*, *124*(3), 147–149.

Wang, Z. Y., P. Larsen, F. Nestmann, and A. Dittrich (1998), Resistance and drag reduction of flows of clay suspensions, *J. Hydraul. Eng.*, *124*(1), 41–49.

Wheatcroft, R. A., and J. C. Borgeld (2000), Oceanic flood deposits on the northern California shelf: Large-scale distribution and small-scale physical properties, *Cont. Shelf Res.*, *20*(16), 2163–2190.

Winterwerp, J. C. (2001), Stratification effects by cohesive and noncohesive sediment, *J. Geophys. Res.*, *106*(C10), 22,559–22,574.

Winterwerp, J. C., and C. Kranenburg (1997), Erosion of fluid mud layers: Experiments and model validation, *J. Hydraul. Eng.*, 512–519.

Wolanski, E., R. J. Gibbs, Y. Mazda, A. Mehta, and B. King (1992), The role of turbulence in the settling of mud flocs, *J. Coastal Res.*, *8*(1), 35–46.

Wright, L. D., C. T. Friedrichs, S. C. Kim, and M. E. Scully (2001), Effects of ambient currents and waves on gravity-driven sediment transport on continental shelves, *Mar. Geol.*, *175*(1–4), 25–45.

E. D'Asaro, Applied Physics Laboratory, University of Washington, 1013 NE 40th Street, Seattle, WA 98195, USA. (dasaro@kraken.apl.washington.edu)

M. P. Lamb, Department of Earth and Planetary Science, University of California, 307 McCone Hall, Berkeley, CA 94720-4767, USA. (mlamb@seismo.berkeley.edu)

J. D. Parsons, School of Oceanography, University of Washington, Box 357940, Seattle, WA 98195-7940, USA. (parsons@ocean.washington.edu)